THE JOURNAL OF PHYSICAL CHEMISTRY C

Article

Cite This: J. Phys. Chem. C 2018, 122, 3617−3627

pubs.acs.org/JPCC

Influence of Microwave Frequency and Power on Nanometal Growth

Bridgett Ashley,[†,‡] Christopher M. Dyer,[†] Jeffery Owens,[‡] and Geoffrey F. Strouse*[,†]

[†]Department of Chemistry and Biochemistry, Florida State University; Tallahassee, Florida 32306-4390, United States

[‡]Air Force Civil Engineer Center, Tyndall AFB, Tyndall AFB, Florida 32403, United States

Supporting Information

ABSTRACT: The rapid heating rates ($\Delta T/\delta t$) achieved in a microwave (MW) reactor has been shown to accelerate reaction rates due to the direct power absorbed (P_{abs}) into the reactants leading to faster kinetics. The P_{abs} is proportional to the dielectric cross section of the materials as defined by the real (ε') and imaginary (ε'') components. In a nanocrystal, the dielectric cross-section will be frequency dependent as well as size dependent. In this work, the frequency dependent growth of nickel nanocrystals at frequencies of 2.45, 15.50, and 18.00 GHz at constant $\Delta T/\delta t$ was studied to evaluate the frequency dependence on MW growth of Ni. A scaling law behavior for growth rates is observed that is shown to depend on the MW electric field strength. A relationship is derived between the "configurational energy" of the precursor molecules and the final nanoparticle size. The study provides a clear description of a microwave effect that is dependent on the frequency and power of the microwave and offers further insight into the physical chemistry of microwave applications to nanomaterial synthesis.

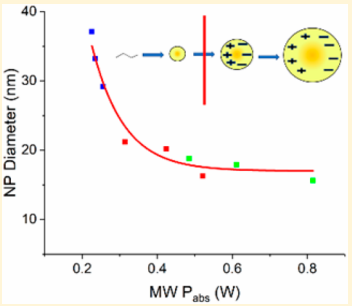

INTRODUCTION

The global desire of reducing energy consumption to produce a more sustainable chemical industry has led to development of more efficient heating methodologies, of which microwave (MW) chemistry is an example. There is no doubt that MW chemistry represents a sustainable industrial process that is significantly more energy efficient.[1,2] Not surprisingly, today MW technology is heavily employed in materials,[3,4] organic,[5,6] peptide,[5] and catalytic chemistry.[2,7]

For much of the past decade, the observation of enhanced reaction rates has led to wide speculation about the physical reason, some based in classical physical chemistry while others are wildly speculative.[8−10] While it has been clearly shown that microwave frequency photons do not possess the energy necessary to cleave even the weakest of chemical bonds,[8,11] several researchers have observed that when a reaction is performed via microwave heating, rather than through convective heat transfer, reaction rates proceed faster than the measured temperature would suggest via the Arrhenius equation.[12] Researchers have rationalized that the accelerated rates arise from the MW creating a more favorable alignment between molecules leading to an increased dielectric constant (chaperone effect)[13,14] or potentially due to raising the vibrational energy of the polar molecules through absorption of the impingent MW electric field, which Richert referred to as configurational temperature.[15−17] In a nanoparticle, a similar condition arises, where the phonon density is perturbed by the presence of a phonon bottleneck condition.[18] The change in configurational energy in the acoustic and optical phonons of a nanoparticle lead to a nonequilibrium perturbation of the phonon distribution. The nonequilibrium distribution leads to a slowing of the cooling rate.[18−20] By analogy, a similar effect will be observed for rotational modes within the nanoparticle, but at much lower energies, allowing the predictions of Richert in microwave molecular heating to be applied to nanoparticles heating in a microwave field.

The nonequilibrium perturbation of the phonon distribution leads to a time dependent increase in configurational energy results from the nanoparticle's inability to instantaneously respond to an outside influence due to phonon confinement. The resultant disequilibrium is realized as the vibrational energy of the molecule being higher than expected given the temperature of the system.[18] In the case of molecular reaction, as discussed by Dudley et al., in a microwave reaction, this can lead to a condition where the more polar solute molecules in the solution have a much higher vibrational energy than the surrounding bath solvent. For a molecule the release energy is near instantaneous, but in an nanometal the energy can give rise to hot electron effects.[19] In both molecular and the nanoparticle cases, the configurational energy would theoretically allow the reaction to proceed faster than expected from Arrhenius law arguments.[16,21] In physics fields, this is also known a fictive temperature, as it cannot be measured by a thermometer, though the phenomenon behaves like a temperature increase.[22]

The magnitude of configurational energy change is dependent on the absorption of the MW field by a molecule, which will be dependent on the frequency and applied power. In a MW cavity this is the electric field strength. Consistent with the configurational energy argument, the observed MW rate enhancement for growth of Ni and Au nanocrystals was directly related to the change in the MW absorption cross-

Received: November 17, 2017
Revised: February 2, 2018
Published: February 5, 2018

DOI: 10.1021/acs.jpcc.7b11366
J. Phys. Chem. C 2018, 122, 3617−3627

section as the nanometal.[23] Kappe demonstrated that MW field strength affects formation of Grignard reagents, irrespective of temperature.[24] The effect of MW power was noted to impact growth rates in II−VI and III−V quantum dots,.[25,26] Vazquez found that higher MW powers (for the same time) in the synthesis of ZnS nanometal resulted in more complete conversion of the precursors, likely resulting from the more rapid decomposition of TTA.[27]

Microwave heating can be treated classically as an alternating EM field passing through a material with any polarizable molecules coupling to the EM field. The early studies show that for a MW reaction, one must consider the effect on thermodynamics and kinetics, and how it is correlated to the amount of energy absorbed (P_{abs}). In analogy to absorption spectroscopy in the visible spectrum, it is convenient to define a penetration depth (D_p) for a reaction system, which is defined in terms of the weighted average of the complex dielectrics for the reaction components. The energy absorbed will produce the latent heat to drive the reaction since $P_{abs} \propto \Delta T/\delta t$. In a typical MW reaction, P_{abs} depends on the applied power at a given frequency for a defined thickness of material. In a nanocrystal the P_{abs} will depend on the nanocrystal size, reflecting the scaling law for the size dependent dielectric.[23,28,29]

Since the dielectric is frequency dependent, the MW frequency is also expected to play a role. In gas phase synthesis the role of MW frequency was observed,[30] but the role of frequency on nanometal nucleation and growth in solution has been largely ignored by the MW chemistry field. The effect on nanometal size using different MW frequencies was investigated by Abe et al, and no frequency dependence was observed for gold nanometal (AuNP) when formed in ethylene glycol—a high MW absorbing solvent.[31] Intriguingly, Abe observed that if oleylamine—a low microwave absorbing solvent—was used, no AuNPs were formed at 2.45 GHz (for 60 W power), but were formed at 5.8 GHz.[31] In CdSe, Massa, et al. observed that size and surface morphology were frequency dependent, with 12 GHz producing the largest nanometal, and frequencies above and below that producing smaller particles.[32] In $BaTiO_2$, Suib, et al. saw that higher frequencies lead to tighter distributions and more spherical particles.[33]

In this manuscript, the influence of both power and frequency on a MW reaction is explored for the growth of Ni nanocrystals from Ni salts using a mild reducing agent. The growth of the Ni follows an autocatalytic growth mechanism allowing the effect of MW power and frequency on the kinetics of the reaction to be systematically evaluated.[23,34] The growth kinetics were followed at three different frequencies (18.00, 15.50, and 2.45 GHz) and three powers chosen to keep the heating rate ($\Delta T/\delta t$) constant for each reaction. The experimental results clearly show the kinetics for nucleation and growth are enhanced by increasing MW field strength. The enhanced reaction rate is due to the increased configurational energy of the system consistent with thermodynamic expectations.

The observation that both frequency and power define the electric field is expected based upon a simple electromagnetic field absorption argument and does not require modification of activation energies or pre-exponential factors. The resultant study lays the foundation for further work to allow the translation of traditional round-bottom convective reactions to MW enhanced reactions. MW enhanced reactions allow efficient scale up of synthetic reactions without the complexity of thermal transport in batch reactors.

EXPERIMENTAL SECTION

Materials. Nickel acetylacetonate ($Ni(acac)_2$), 70% oleylamine (OAm), and 90% oleic acid (OA) were purchased from Sigma−Aldrich. Paraffin wax and solvents were used without further purification.

Synthesis of Ni NP. A 7.50−18.00 GHz multimode cavity (16 cm cube) of aluminum with mode stirrer was attached to a IFI traveling wave tube amplifier, model 188-500, capable of producing 7.50−18.00 GHz microwave radiation, with a WRD 750 waveguide was used for the 15.50 and 18.00 GHz synthesis. The TWTA was driven by an Anritsu MG3692C signal generator. The top of the multimode cavity was modified to hold CEM 10 mL tubes and CEM fiber optic thermometer. Additionally, a single mode resonant cavity (TE_{015}) coupled to a Gerling MW source was used for the 2.45 GHz synthesis.

Spherical *fcc*-NiNPs were synthetically prepared using MW-assisted decomposition of $Ni(acac)_2$ in 0.01 M solution of $Ni(acac)_2$ in OAm. The synthetic preparation of the *fcc*-Ni was carried out by mixing 5.0 mmol of $Ni(acac)_2$ and 500 mL of OAm in a round-bottom flask and degassing under vacuum at 90 °C. A 5 mL aliquot of the clear blue solution was transferred under ambient conditions into a 10 mL borosilicate CEM MW vessel and capped. No stir bar or inert atmosphere was used in the reaction vessel. The solution was irradiated until 240, 260, and 280 °C and until reaction completion in either the TWTA multimode or the Gerling single mode cavity. Temperature and power were monitored actively during the reaction.

Characterization. The NiNPs were fully characterized by pXRD and TEM (Figure S1).The NiNPs can be indexed to the *fcc* structure (card 98−002−2027) measured on a Panalaytical Empyrion powder X-ray diffractometer (using Cu Kα λ = 1.5418 Å radiation). The size, size dispersity, and morphology were measured by transmission electron microscopy (TEM) with a JEM-ARM200cF electron microscope at 200 kV accelerating voltage. Diluted NP samples were drop-cast from dispersion in toluene onto 300-mesh copper grids and left to dry under reduced pressure overnight. Histograms generated from image capture of >300 nanoparticles in ImageJ was used to generate the size distribution curves. Solution absorption spectra used for the growth kinetics were obtained using a Varian Cary 50 UV−visible spectrophotometer in a 1 cm quartz cuvette from 400 to 1000 nm.

RESULTS AND DISCUSSION

Effect of Microwave Frequency and Power. The absorption of the MW field will be dependent on the complex dielectric $\varepsilon^* (=\varepsilon' - i\varepsilon'')$, which is often expressed in terms of the dielectric loss function $\tan \delta = \varepsilon''/\varepsilon'$. The P_{abs} will scale with the concentration of molecules in solution that have significant dielectric loss, and in a dilute reaction is analogous to the absorption of EMR radiation, and will follow Beer−Lambert law behavior. It is important to remember that the energy of a MW photon is not sufficient to break bonds or excite electrons, but rather generates heat by molecular friction as the dipole reorients with the oscillating field. The absorption of the MW field will be dependent on the complex dielectric $\varepsilon^* (=\varepsilon' - i\varepsilon'')$, which is often expressed in terms of the dielectric loss function $\tan \delta = \varepsilon''/\varepsilon'$. The MW cross-section which is correlated to the absorbed power (P_{abs}) will scale with the MW

DOI: 10.1021/acs.jpcc.7b11366
J. Phys. Chem. C 2018, 122, 3617−3627

frequency, the concentration of molecules in solution, and in a dilute reaction should follow Beer–Lambert law behavior analogously to the absorption of EMR radiation. Since each material will have a unique electromagnetic absorption and scattering cross section, a solution or mixture can experience selective heating, which impacts the rate of heating and, therefore, the overall kinetics of the reaction.

During the growth of Ni (Figure 1A), the MW field is primarily absorbed into the OAm early in the reaction and as

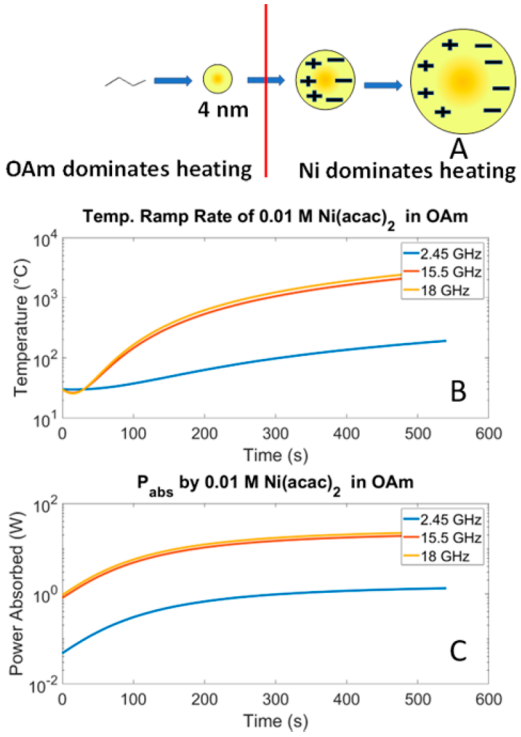

Figure 1. (A) Illustration of when reaction goes from microwave absorption dominated by oleylamine to nickel nanoparticles. (B) Temperature vs time for reaction at different frequencies, and (C) power absorbed for reaction at different frequencies. Parts B and C both assume a steadily growing nanoparticle, and a constant E_0.

the reaction progresses, the absorption will become a weighted average of the OAm and the size dependent Ni dielectric value. The increasing absorption of the MW field by the growing Ni nanocrystal is anticipated to scale with the Ni size[35,36] increasing the configurational energy of the Ni surface when the Ni nucleates due to confinement effects on the electron–phonon properties of nanomaterials.

For a metal the dielectric dispersion generally increases with increasing MW frequency, and therefore an increase in heating rate is anticipated at higher MW frequencies reflecting the increase in P_{abs}. The ramp rate $(\Delta T/\delta t)$ for the reaction can be calculated by equating the absorbed MW power (P_{abs}) to the calorimetric equation

$$P_{abs} = M\frac{dC_p}{dt}\frac{\Delta T}{dt} = \left(\frac{1}{2}\omega\varepsilon_0\frac{d\varepsilon''_{eff}}{dt}\int_V (\vec{E}^* \times \vec{E})\, dV\right) \quad (1)$$

where M is the mass, C_p is the specific heat capacity, ΔT is the change in temperature, t is time, ω is frequency, ε_0 is the permittivity of free space, ε'_{eff} is the lossy permittivity of the material, V is volume, E^* is the complex conjugate of the electric field, and E is the electric field. ε'_{eff} is a frequency-dependent term. For a metal the dielectric dispersion generally increases with increasing MW frequency, and therefore an increase in heating rate is anticipated at higher MW frequencies. In the case of autocatalytic Ni nanometal growth, eqs 1-2 can be used to predict the reaction temperature and absorbed energy as a function of frequency with respect to the changing size-dependent dielectric of the Ni NP growing with time, and the evolving heat capacity of the system.[28,29,37]

$$\varepsilon^* = 1 + \frac{m^* k_F (2r)^2}{20\pi^2 a_B} + \frac{139}{1200\pi^2 a_B}\left(2 + i\frac{\omega m^* k_F (2r)^3}{6\hbar}\right) \quad (2)$$

Here k_F is the Fermi level, m^* is the effective electron mass, r is the nanoparticle radius, and a_B is the Bohr radius. Figure 1 assumes a constant electric field (E_0) throughout the reaction. The dip in the temperature plot (Figure 1B) arises from the change in heat capacity for OAm with increasing temperature prior to growth of the Ni nanometals to a size regime in which MW absorption begins to play a substantive role.

Using the values in Table 1, a theoretical plot of the frequency dependent reaction temperature vs time is shown in Figure 1B. The dip in the temperature plot arises from the change in heat capacity for OAm with increasing temperature competing with the increasing contribution from the growing Ni nuclei. The dielectric loss values for the reaction components used in eq 1 are extracted experimentally using a vector network analyzer (VNA) and are listed in Table 1. Figure 1C is a theoretical plot of P_{abs} for each frequency can also be generated. From the P_{abs} plot the effective evolution of MW absorption by the reaction constituents can be envisioned by taking into account the number of nuclei, the size dependent dielectric for Ni, and the decreasing C_p for the solvent with increasing reaction temperature. Inspection of parts B and C of Figure 1 leads to the observation that, during the reaction, OAm will dominate the heating profile initially until the Ni nanoparticle grow to sizes >4 nm. At this point the MW absorption will steadily shift from OAm to Ni, as the weighted average of OAm absorption and absorption by the Ni, which scales with size and concentration.

Table 1. Dielectric Loss (ε'') for the Reaction Precursors at the Three Microwave Frequencies Used in the Experiments

	2.45 GHz	15.5 GHz	18 GHz
oleylamine	0.102 ± 0.011	0.207 ± 0.008	0.238 ± 0.014
$Ni(acac)_2$	0.001 ± 0.004	0.012 ± 0.010	0.011 ± 0.009
Ni (4 nm)	0.010[a]	0.063[a]	0.073[a]
Ni (6 nm)	0.034[a]	0.212[a]	0.247[a]

[a]Calculated values.

Frequency Dependent Reaction Rates. Nanometal growth at subsaturation conditions from metal salts in solution to form metal nanoparticles is well described by the autocatalytic growth process, wherein the growing seed acts as a surface mediated catalyst thus accelerating the reaction rate as the nanoparticle grows.[23,34,38–60] In the autocatalytic mechanism growth onto a nuclei surface occurs faster than continuous nucleation steps leading to a lag growth behavior but tight size distributions. In the case of Ni nanoparticles growth by the mild reduction of $Ni(acac)_2$ with OAm has been shown to follow an autocatalytic process, where the first step of the reaction is governed by formation of the reduced Ni

DOI: 10.1021/acs.jpcc.7b11366
J. Phys. Chem. C 2018, 122, 3617–3627

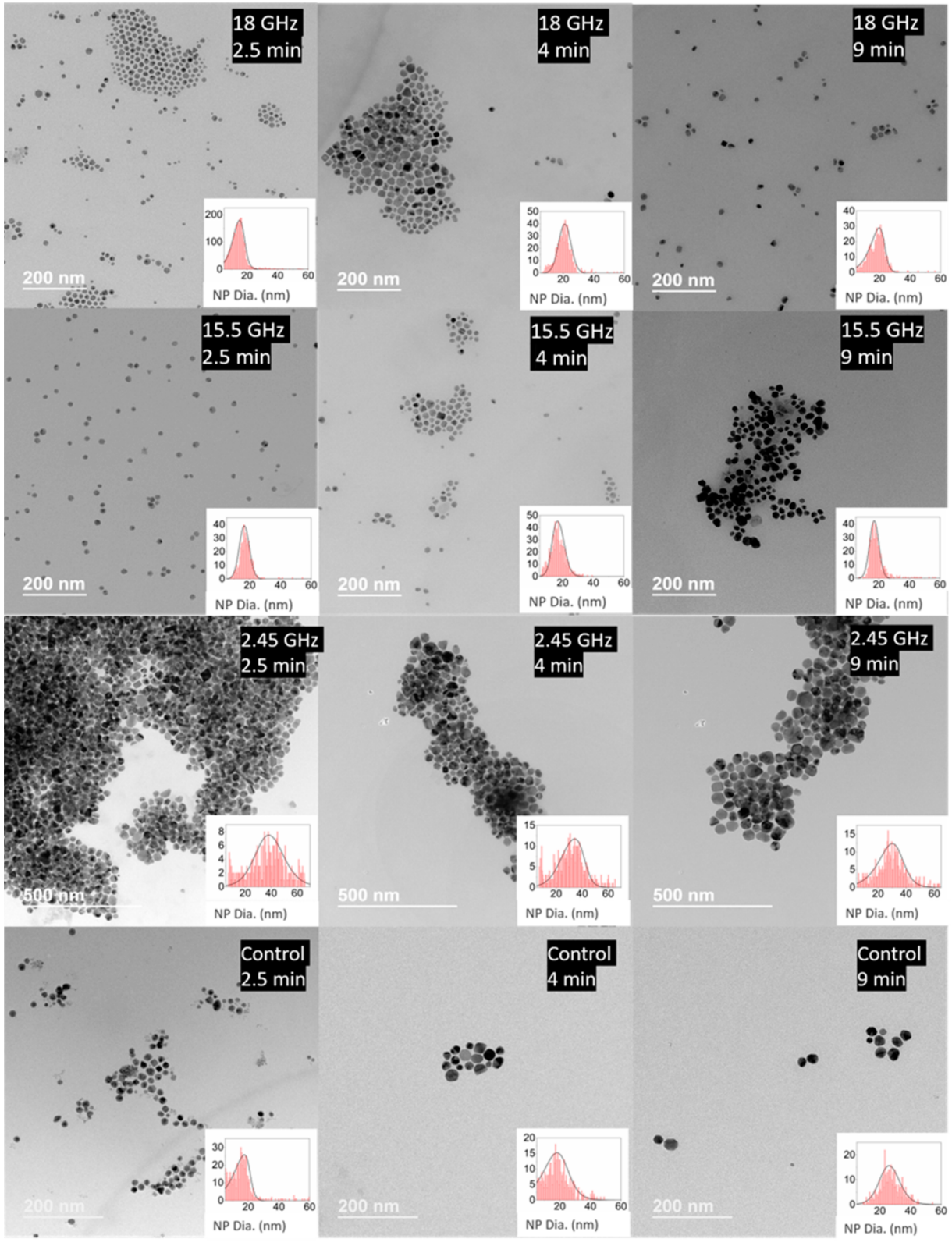

Figure 2. TEMs of the nanoparticles formed in the MW at 18.00, 15.50, and 2.45 GHz, and control experiments. Histograms are based on >300 particles.

precursor and nucleation ($Ni(acac)_2 \rightarrow Ni_0$) and the second step is the continuous growth of the nucleus ($Ni_0 \rightarrow \rightarrow \rightarrow$ NiNP) when carried out at non- exponential behavior of an autocatalytic saturated conditions.[23,34] Tilley showed that nickel nanoparticle growth from $Ni(acac)_2$ follows this two-step growth in conventional thermal reactions,[34] and our previous work showed that similar reactions follow the FW mechanism in microwave thermal reactions.[23]

The initial step in the autocatalytic reaction is governed by the rate k_1 and the second step governed by the rate k_2 and will

DOI: 10.1021/acs.jpcc.7b11366
J. Phys. Chem. C 2018, 122, 3617−3627

follow classical Arrhenius law behavior ($k_1 = Ae^{E_a/RT}$).[38,39] In both cases the rates will follow reactions, which in turn allows the prediction that a significant acceleration of reaction rate will occur at higher MW frequencies due to larger values for P_{abs} and, by inference, more efficient heating.

In addition to a rate enhancement, the size dispersity will also be influenced in an autocatalytic reaction. In the autocatalytic mechanism the ratio of $k_2[Ni^0]/k_1$ is defined as the *R*-factor and as shown in our previous study to dictate the size distribution.[23] The power dependent autocatalytic growth R_{FW} value was previously reported to follow the empirical law for size $y = -0.0026(x) + 26.4$ (x = power applied; y = size) and for distribution $z = -0.034(x) + 60.1$ (x = power applied; z = dispersion).[23] Therefore, carrying out the MW growth of a material that follows autocatalytic growth at higher frequency should lead to faster reaction times, smaller nanocrystals, and tighter size dispersions.

To evaluate the hypothesis, the MW frequency dependence of the Ni growth reaction rates (k_1 and k_2), size, and size dispersity were tested using 5 mL of 0.01 M $Ni(acac)_2$ in OAm solution in a MW cavity operating at constant power to ensure constant heating rates $\Delta T/\delta t$ (ΔT of 250 °C in 9, 4, and 2.5 min) at 2.45 GHz (140, 148, and 160 W), 15.50 GHz (138, 174, and 232 W), and 18.00 GHz (91, 123, 151 W).

Powder X-ray diffraction of the samples confirm the isolation of *fcc*-Ni in all reactions (Figure S1). The size and size dispersity of the isolated Ni nanocrystals are shown in Figure 2, where it can be seen that for each frequency, the size decreased and the size dispersion narrowed as the power increased. The TEM show well-formed nanocrystals across all frequency and $\Delta T/\delta t$ conditions. The size dispersity plots in Figure 2 show evidence of Ostwald ripening at all-time points for the convective reaction (control) and at long reaction times, as expected.

The results of the growth study in Figure 2 are revealing when compared to the theoretical plots in Figure 1, where a change in absorption of the microwave field by the reactants will increase by 2 orders of magnitude leading to more rapid heating as the frequency is increased from 2.45 to 18 GHz. The effect of increased absorption can be seen in Figure 3A, where the size vs $\Delta T/\delta t$ is plotted. The plot shows a clear decrease in nanoparticle size with increasing $\Delta T/\delta t$ and the largest nanocrystals are observed for the lowest applied frequency. However, there is no immediately apparent correlation between size and applied frequency as the 18 GHz data is larger than the 15 GHz Ni sizes and much smaller than the 2.45 GHZ samples at a $\Delta T/\delta t$ of 0.5. While surprising, the answer lies in the kinetics of the growth mechanism for a mild reducing reaction carried out at subsaturation conditions. As shown previously,[23,34,40−42] the subsaturation conditions lead to an autocatalytic mechanism of growth rather than the classical nucleation mechanism employed at supersaturation.

The Finke−Watzky (F−W) autocatalytic mechanism is unique from a classical nucleation mechanism. In this mechanism, there is a slow nucleation step whose rate (k_1) is dependent on the slow reduction of Ni^0 monomers from the Ni salt,[34,43−45] followed by a rapid, self-catalyzed nanoparticle growth step characterized by k_2. Unlike a classical nucleation mechanism, in the autocatalytic mechanism the initial metal monomer M^0 concentration is below saturation. This leads to the number of nuclei formed at the start of the autocatalytic part of the reaction to be invariant if $k_1 \ll k_2$. In our previous work we showed the number of nanoparticle nuclei formed at

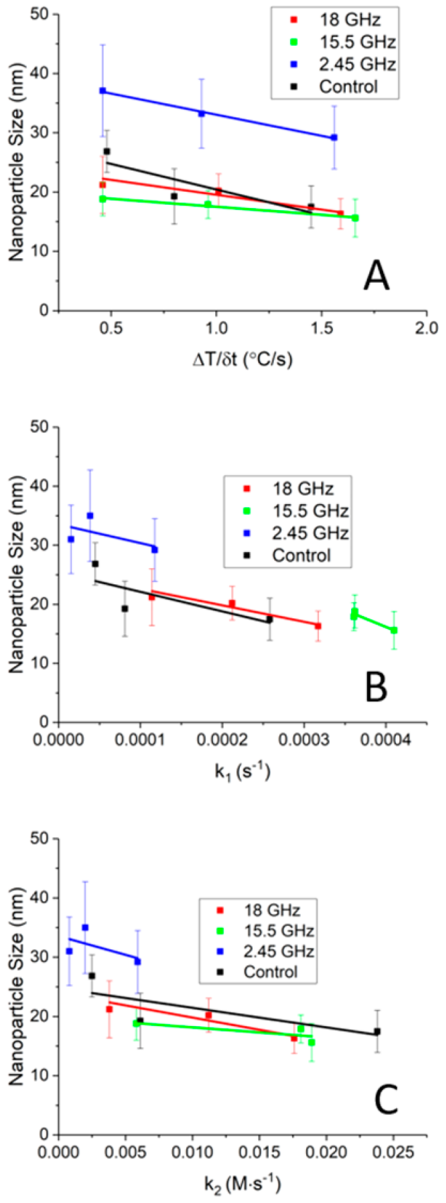

Figure 3. Plots of nanoparticle size vs (A) $\Delta T/\delta t$ of reaction, (B) k_1 of reaction, and (C) k_2 of reaction. $N = 2$ for all.

240 °C was within experimental error of the number of nanoparticles at the end of the reaction.[23] It has also been shown that when $k_1 \ll k_2$, k_1 and k_2 are separated in time and are distinct.[46−48] It has been disputed that k_1 is not sufficiently suppressed to have distinct nucleation and growth without invoking a mechanism different from autocatalysis.[49,50] Xia et al., on the other hand, have shown clearly that the autocatalytic step is sufficient to suppress nucleation.[51] In the case of microwave assisted nanoparticle synthesis, it could be hypothesized that the point at which the nanoparticle is large enough to dominate the MW absorption over the precursors is the point at which k_1 transitions to k_2,[23] though more work needs to be done to elucidate this.

The autocatalytic mechanism has been fully demonstrated to explain the growth behavior for nano metal growth at sub saturation conditions.[23,34,38−60] While the FW mechanism is simplified to a 2-step process, it is the simplest model for fitting sigmoidal nanoparticle nucleation and growth data,[52−54]

DOI: 10.1021/acs.jpcc.7b11366
J. Phys. Chem. C 2018, 122, 3617−3627

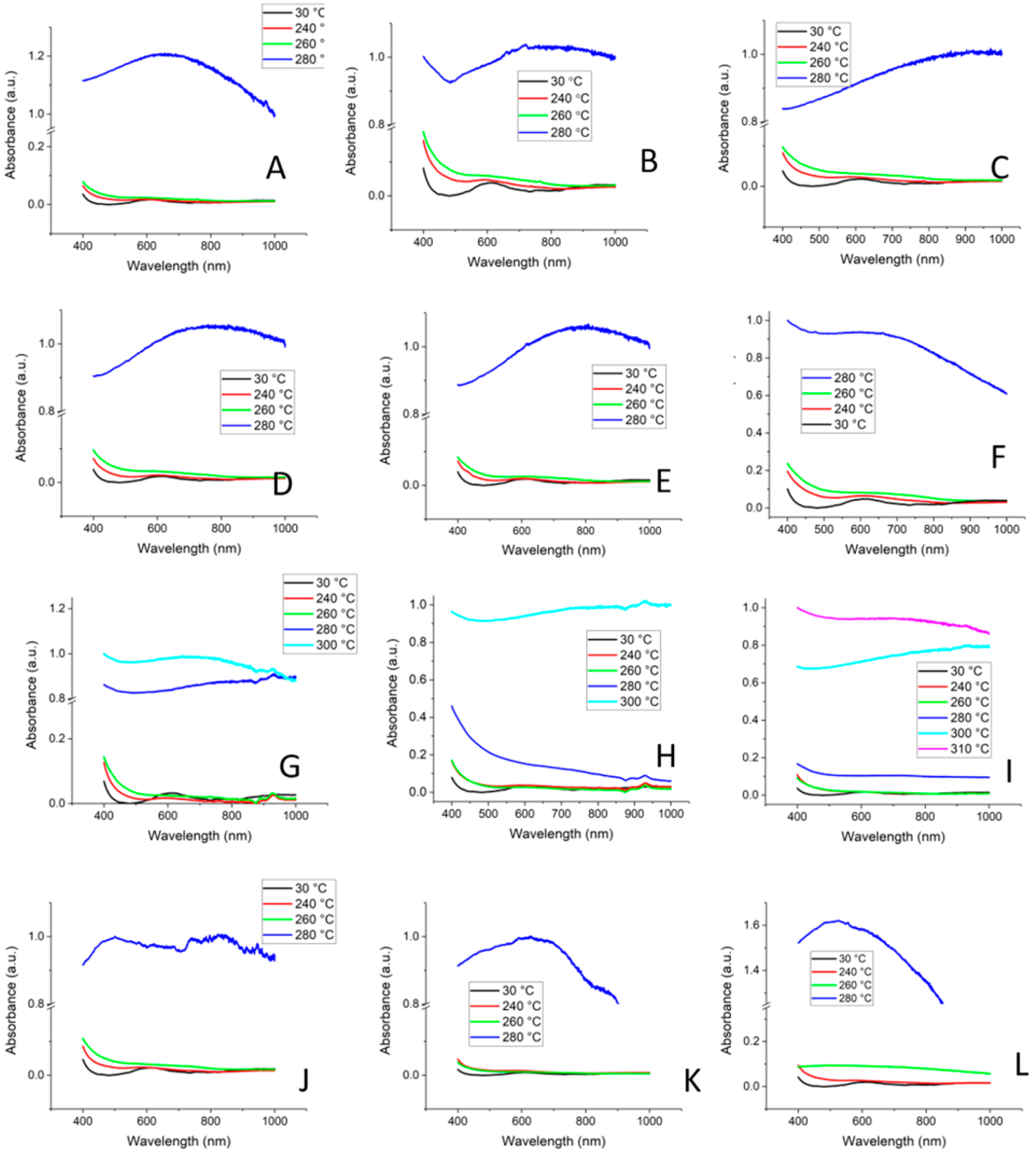

Figure 4. UV−vis spectra for all experiments: (A) 18 GHz, 2.5 min; (B) 18 GHz, 4 min; (C) 18 GHz, 9 min; (D) 15.5 GHz, 2.5 min; (E) 15.5 GHz, 4 min; (F) 15.5 GHz, 9 min; (G) 2.45 GHz, 2.5 min; (H) 2.45 GHz, 4 min; (I) 2.45 GHz, 9 min; (J) control, 9 min; (K) control, 4 min; (L) control, 2.5 min. $N = 2$ for all.

including that of NiNPs grown in mild reducing conditions.[34,46] As the manuscript is focused on MW flux, we have adapted this model to explain the power and frequency dependent growth behavior. Within this assumption the rate of Ni formation (d[NP]/dt) can be expressed as

$$\frac{\mathrm{d}}{\mathrm{d}t}[\mathrm{NP}] = -k_1[\mathrm{M\ salt}] + k_2[\mathrm{M\ salt}][\mathrm{M}^*] \tag{3}$$

The autocatalytic mechanism has been fully described for formation of Ag,[55,56] Au,[38,57−59] Ru,[39] and Ni[34] in convective reactions and demonstrated to describe growth of Ag,[60] Ni,[23] and Au[23] in a MW reactor.

The frequency dependent growth at fixed heating rates ($\Delta T/\delta t$) for the mild reduction of $Ni(acac)_2$ to form Ni nanocrystals was monitored using UV−vis absorption spectroscopy at fixed time points to follow the increase in Ni dielectric absorption, which is broad and featureless, and the loss of the $Ni(acac)_2$ absorptions at 610 nm and a rising absorption above 420 nm (Figure 4). In Figure 5, the Ni formation rate (d[NP]/dt) is plotted by measuring the change in absorption intensity at 488 nm, where no $Ni(acac)_2$ absorption exists and as shown previously corresponds to absorption by only the Ni nanocrystals.[23] In Figure 5, the change in absorption at 488 nm is fitted to the sigmoidal growth curve behavior for a classical autocatalytic mechanism.

In the autocatalytic mechanism, the value for [M*] at the end of nucleation is assumed to be equivalent to the number of nanometal particles in the reaction at t_∞, as was shown

DOI: 10.1021/acs.jpcc.7b11366
J. Phys. Chem. C 2018, 122, 3617−3627

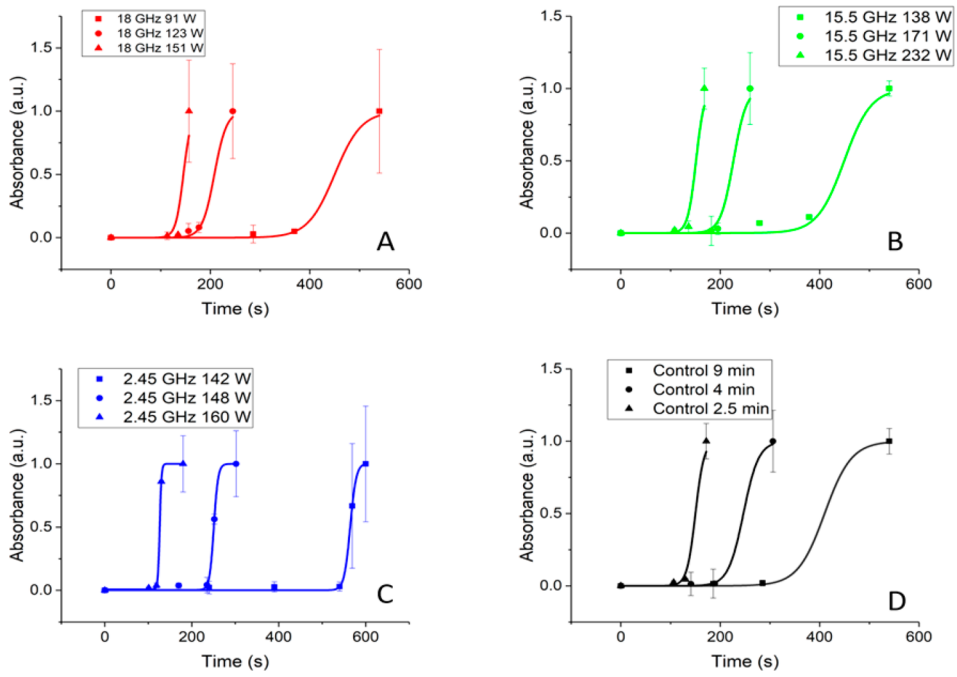

Figure 5. Plot of 488 nm absorbance for all reactions showing the classic sigmoidal curve of Finke–Watzky kinetics. $N = 2$ for all.

Table 2. Frequencies, Powers, E_0, Nanoparticle Size, and Absorbed Power for each of the Nine MW Experiments[a]

freq (GHz)	time (min)	dissipated MW power (W)	E_0 (V/m)	NP diameter (nm)	k_1 (s^{-1})	k_2 ($M{\cdot}s^{-1}$)	N of Ni nanoparticles
18.00	9	91	6.23×10^4	21.2 ± 9.6	$1.141 \times 10^{-4} \pm 1.05 \times 10^{-4}$	0.0058 ± 0.00488	8.38×10^{17}
18.00	4	123	7.24×10^4	20.2 ± 5.7	$2.12 \times 10^{-4} \pm 1.37 \times 10^{-4}$	0.0112 ± 0.00374	4.80×10^{17}
18.00	2.5	151	8.02×10^4	16.3 ± 5.1	$3.17 \times 10^{-4} \pm 1.79 \times 10^{-4}$	0.0176 ± 0.00403	2.58×10^{18}
15.50	9	138	7.96×10^4	18.8 ± 5.6	$4.62 \times 10^{-4} \pm 4.72 \times 10^{-5}$	0.0058 ± 5.2010^{-4}	4.75×10^{17}
15.50	4	174	8.94×10^4	17.9 ± 4.7	$3.61 \times 10^{-4} \pm 2.05 \times 10^{-4}$	0.0181 ± 0.00249	1.51×10^{18}
15.50	2.5	232	1.03×10^5	15.6 ± 6.4	$4.1 \times 10^{-4} \pm 1.98 \times 10^{-4}$	0.0189 ± 0.00142	2.11×10^{18}
2.45	9	140	1.64×10^5	35.1 ± 11.6	$3.85 \times 10^{-4} \pm 2.07 \times 10^{-4}$	0.02 ± 0.0022	1.49×10^{17}
2.45	4	148	1.68×10^5	30.7 ± 15.5	$1.52 \times 10^{-5} \pm 2.06 \times 10^{-4}$	0.0008 ± 0.00213	1.42×10^{17}
2.45	2.5	160	1.74×10^5	29.2 ± 10.6	$1.176 \times 10^{-4} \pm 1.08 \times 10^{-4}$	0.0059 ± 0.00493	1.96×10^{17}
control	9	N/A	N/A	26.8 ± 7.15	$4.5 \times 10^{-5} \pm 1.01 \times 10^{-4}$	0.0025 ± 0.008	7.00×10^{17}
control	4	N/A	N/A	19.3 ± 9.34	$6.7 \times 10^{-5} \pm 2.89 \times 10^{-4}$	0.0061 ± 0.028	2.71×10^{18}
control	2.5	N/A	N/A	17.5 ± 7.09	$2.4 \times 10^{-4} \pm 6.34 \times 10^{-5}$	0.0238 ± 0.006	1.38×10^{18}

[a] E_0 is based on the power measured in the cavity, not the set power of the instrument. For the TWTA these are the same, but for the Gerling, due to the water dump, the measured power is ~10% of the set power. Here, 9, 4 and 2.5 min are the times from room temperature to 280 °C, which directly correspond to the powers listed in the second column.

previously,[23] and as detailed in the Supporting Information (Figure S2) for this paper.

The number of nanometal particles is extracted from the absorption data at 488 nm using the Ni extinction values for the isolated TEM sizes at the completion of the reaction and the numbers are listed in Table 2, along with the values for k_1 and k_2.[23,61−63] The number of Ni nanoparticles is calculated by treating the extinction (absorption) cross-section for a metal as a size dependent dielectric using Mie scattering to find the size dependent extinction cross-section[61]

$$\sigma_{ext} = \frac{9V\epsilon_m^{3/2}}{c} \times \frac{\omega\epsilon_2}{[\epsilon_1 + 2\epsilon_2]^2 + (\epsilon_2)^2} \quad (4)$$

where V is the volume of the nanoparticle, εm is the dielectric of the medium, assumed to be invariant with frequency, c is the speed of light, ω is the frequency being absorbed, and ε_1 and ε_2 are the frequency dependent real and imaginary parts of the dielectric of the nanoparticle, respectively. The number of nanoparticles will be related to the absotption intensity through the extinction cross-section in analogy to Beer's law[62]

$$A = \sigma_{ext} bN \quad (5)$$

where b is the path length of the cell and N is the number of nanoparticles per unit volume. The concentration of nanoparticle is critical in predicted the rate law behavior for the assumed autocatalytic mechanism.

Using eq 3[23,40] the values for k_1 (nucleation) and k_2 (growth) are extracted and plotted in Figure 3, parts B and C, as a function of the nanoparticle size extracted from the TEM data.[23,34] The experimental conditions and the kinetic parameters are summarized in Table 2. The values of k_1 and k_2 exhibit no immediate correlation with the applied frequency, albeit a linear decrease is observed in k_1 and k_2 for a given frequency and the general behavior of the frequency dependence mimics the $\Delta T/\delta t$ plot in Figure 3A.

DOI: 10.1021/acs.jpcc.7b11366
J. Phys. Chem. C 2018, 122, 3617−3627

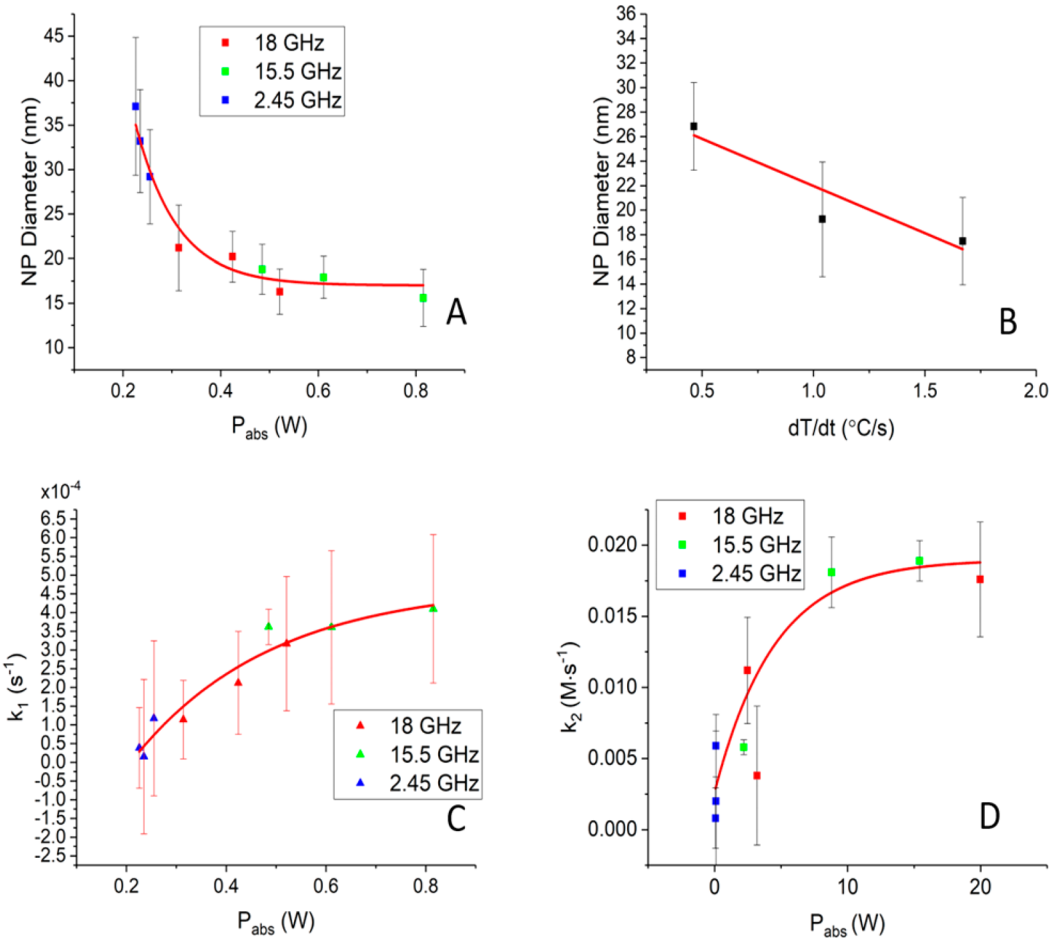

Figure 6. (A) Plot of Ni NP size vs absorbed power calculated using eq 4. (B) Plot of control Ni NP made in Al block vs dT/dt. (C) Plot of k_1 vs P_{abs} by the reaction at the beginning of the reaction and D) k_2 vs P_{abs} by the reaction when the NP are 4 nm in diameter.

To develop a model that allows the observed frequency dependent behavior for autocatalytic growth of Ni in a MW cavity, the configurational energy of the reaction, which is related to the power absorbed (P_{abs}) by the reactants, must be considered. Richert showed theoretically that the configurational energy of molecules interacting with an impingent MW electric field will be a function of both power applied and the frequency.[15,64] The configurational energy difference is proportional to the power absorbed divided by the heat capacity of the molecule.

$$\frac{\tau P_{abs}}{\Delta c_p} = \frac{\varepsilon_0 {E_0}^2 \Delta\varepsilon}{2\Delta c_v}\left(\frac{\omega^2\tau^2}{1+\omega^2\tau^2}\right) \tag{6}$$

where E_0 is the strength of the electric field in the cavity (dependent on power and frequency of the MW, as well as the dimensions of the cavity), $\Delta\varepsilon$ is the dielectric strength (the static dielectric constant minus the dielectric constant at very high frequencies), Δc_v is the slow mode part of the volumetric specific heat (approximated as $^1/_2$ the volumetric specific heat), Δc_p is the slow mode part of the specific heat (approximated as $^1/_2$ of the specific heat), ω is the frequency in radians, and τ is the relaxation time of the molecule. E_0 is determined from the power, frequency and volume of the cavity (if cubic or rectangular multimodal with mode stirrer) using

$$E_0 = E_{rms} = \left(4\frac{(P/V)Q}{\omega\varepsilon_0}\right)^{1/2} \tag{7}$$

where P is the power dissipated in the system, V is the volume of the cavity, and Q is the quality factor of the cavity, which can be estimated by $2V/\sigma S$, where σ is the skin depth of the cavity at frequency ω, and S is the surface area of the inside of the cavity. For a single mode cavity (TE_{10n}), where the power is not uniformly distributed, $E_0 = \sqrt{2} \times E_{rms}$. The relaxation time ($\tau$) of the molecule can be calculated from the Debye equation,

$$\varepsilon^* = \varepsilon_\infty + \frac{\varepsilon_\infty - \varepsilon_s}{1 + i\omega\tau} \tag{8}$$

The relaxation time can be extracted from the slope of a linear Cole−Cole plot of ε' vs ε''/ω, where ε' and ε'' are taken from VNA measurements (Table 2).[65] Inspection of eqs 4−6 shows that the configurational energy will be small, since τ will be in picoseconds and E_0 will be ~10^5 V/m, leading to P_{abs} of ~10^{-3} W.

In Figure 6, a clear trend is noticeable in the plot of the P_{abs} vs the nanometal size isolated in the MW reaction. The P_{abs} exhibits an exponential scaling law behavior for MW absorption by the Ni. The scaling law behavior can be rationalized since $P_{abs} = P_o(e^{-2\alpha^d})$, where P_o is the initial power, α is the size dependent MW attenuation, and d is the diameter. The value of α scales as the size dependent dielectric constant as shown previously.[23,37,57,61,63,66] This provides a reasonable explanation

DOI: 10.1021/acs.jpcc.7b11366
J. Phys. Chem. C 2018, 122, 3617−3627

of the observed dependence on MW power applied and frequency observed in the Ni reactions. If there were no MW influence, we would expect to see only three sizes of NP, one for each of the $\Delta T/\delta t$'s. This assumption is clearly demonstrated by inspection of Figure 6B, where control experiments were performed under identical conditions to the MW studies with CEM tubes in an aluminum block at identical heating rates ($\Delta T/\delta t$). A description of the setup is shown in Figure S3. The convective control experiments do not exhibit an exponential dependence on growth.

In parts C and D of Figure 6, the P_{abs} argument is correlated with the rates from autocatalytic growth. The rate behavior for k_1 and k_2 exhibit exponential behavior, with k_2 being more sensitive to $P_{abs.}$ Previous studies on MW autocatalytic reactions have suggested MW absorption is predominately in k_2 consistent with the increasing MW absorption as the nanocrystal grows.[60] It should be noted that the curve fitting for k_2 is much poorer than for k_1 or for Figure 6A. This is not unexpected due to the pseudo elementary nature of k_2, as k_2 is in reality a composite rate dictated by surface area that changes as the nanoparticle grows.[47] It should also be noted that since k_2 is one to 2 orders of magnitude higher than k_1. Even if nucleation continued during k_2, it would be approximately 1−3% of the rate, as well as being a competing mechanism for nickel ion consumption. This level of precision is unresolvable in the data presented in this paper.

Since both reaction rates are expected to follow the Arrhenius equation, we can extract the E_a and Arrhenius prefactor (A) for both the nucleation event and autocatalytic growth (using power instead of temperature) from the plots (Figure 6 C and D). The Arrhenius law fits yield values for k_1 of $E_a^{(1)}/R$ = 0.869 kJ·W/mol with an $A^{(1)}$ of 16.1 × 10^{-4} s^{-1}, while for k_2 an $E_a^{(2)}$/R of 0.162 kJ·W/mol and an $A^{(2)}$ of 115.2 × 10^{-4} $s^{-1}$is measured. The experimentally observed Arrhenius law behavior confirms the reactions follow classical thermodynamic behavior. The observation that the MW enhancement is explainable within thermodynamic models, indicates that the MW effects should be expressed in terms of MW absorption by the reactants or, in other words, the MW flux as defined by applied power/frequency.

CONCLUSIONS

In nanometals, it is clear that MWs do not break bonds, and do not change thermodynamic or kinetics; however, MW enhancement can be observed. In this paper, the effect of the MW applied power and frequency at constant $\Delta T/\delta t$ is explored for Ni growth under autocatalytic conditions. The results show a scaling law behavior with size due to the increasing MW cross section of the growing nanometal. The increased P_{abs} that occurs is understood in terms of local energy changes. Demonstrating a correlation of MW enhancement being related to thermodynamics and not nonthermal MW effects is critical to understanding experimental reports on MW accelerated growth. This leads to the conclusion that a generalized strategy for reaction design would be to optimize concentration and applied power at a given frequency to achieve the desired particle size and size distribution since P_{abs} is dependent on reaction concentrations of precursors.

The study shows definitively that the reaction rate for nanometal growth is a problem of electromagnetic radiation absorption and thus will be dependent on the applied power, frequency, relaxation time, and concentration of the reactants. It is believed this strategy can be applied to organic reactions to explain rate acceleration, although the magnitude of the change in P_{abs} may mask the kinetic effects. It is hoped that continued exploration of MW enhancement using physical chemistry will allow reactions to be translated efficiently from a convective format to a MW format with minimal guesswork. This would lead to substantial energy savings[1,2] due to the higher efficiency of a MW volumetrically heating when compared to convective reactors.

While this work does not disprove "nonthermal" MW effects, it provides a physical description supported by kinetics and thermodynamic evaluation to understand how selective molecular MW heating can explain differences in reaction rates and reaction products commonly seen in microwave chemistry and commonly referred to as "nonthermal" MW effects. The science of microwave chemistry can only be enhanced by a greater understanding within the scientific community of the importance of applying EM physics to the understanding of chemical reactions.

ASSOCIATED CONTENT

Supporting Information

The Supporting Information is available free of charge on the ACS Publications website at DOI: 10.1021/acs.jpcc.7b11366.

Detailed figures of setup and additional supporting images for the characterization of the Ni samples are provided (PDF)

AUTHOR INFORMATION

Corresponding Author

*(G.F.S.) E-mail: strouse@chem.fsu.edu.

ORCID

Geoffrey F. Strouse: 0000-0003-0841-282X

Author Contributions

B.A. measured the power-dependent MW reactions, carried out the dielectric measurements and theoretical derivations and assisted in the writing of the manuscript. C.D. characterized the power-dependent MW reactions. J.O. assisted in the experimental design and interpretation. G.F.S. designed the project and assisted in interpretation and conclusions and in the writing of the manuscript. All authors revised the manuscript.

Notes

The authors declare no competing financial interest.

ACKNOWLEDGMENTS

We (G.F.S. and B.A.) wish to thank the National Science Foundation for Grant CHE-1608364, "SusChEM: Understanding Microwave Interactions to Control Magnetic Nanocrystal Growth from a Single Source Precursor". This project was supported (B.A., J.O.) in part by an appointment to the Research Participation Program at the Air Force Civil Engineer Center administered by the Oak Ridge Institute for Science and Education. The TEM imaging at FSU is supported by the Florida State University Research Foundation, and through the National High Magnetic Field Laboratory National Science Foundation Cooperative Agreement DMR-1157490, the State of Florida, and Florida State University. The authors would also like to thank Parth Vakil for all the TEM work he did for this article.

DOI: 10.1021/acs.jpcc.7b11366
J. Phys. Chem. C 2018, 122, 3617−3627

REFERENCES

(1) Razzaq, T.; Kappe, C. O. On the Energy Efficiency of Microwave-Assisted Organic Reactions. *ChemSusChem* **2008**, *1*, 123−132.

(2) *Microwave Heating as a Tool for Sustainable Chemistry*; Leadbeater, N. E., Ed.; Taylor and Francis Group: Boca Raton, FL, 2010.

(3) Gerbec, J. A.; Magana, D.; Washington, A.; Strouse, G. F. Microwave-Enhanced Reaction Rates for Nanoparticle Synthesis. *J. Am. Chem. Soc.* **2005**, *127*, 15791−15800.

(4) Mohamed, M. B.; AbouZeid, K. M.; Abdelsayed, V.; Aljarash, A. A.; El-Shall, M. S. Growth Mechanism of Anisotropic Gold Nanocrystals via Microwave Synthesis: Formation of Dioleamide by Gold Nanocatalysis. *ACS Nano* **2010**, *4*, 2766−2772.

(5) Kappe, C. O. Controlled Microwave Heating in Modern Organic Synthesis. *Angew. Chem., Int. Ed.* **2004**, *43*, 6250−6284.

(6) Hajek, M. Microwave Catalysis in Organic Synthesis. *Microwaves in Organic Synthesis* **2002**, 345−378.

(7) Hunt, J.; Ferrari, A.; Lita, A.; Crosswhite, M.; Ashley, B.; Stiegman, A. Microwave-specific enhancement of the carbon−carbon dioxide (Boudouard) reaction. *J. Phys. Chem. C* **2013**, *117*, 26871−26880.

(8) de la Hoz, A.; Diaz-Ortiz, A.; Moreno, A. Review on Non-Thermal Effects of Microwave Irradiation in Organic Synthesis. *J. Microw. Power Electromagn. Energy* **2006**, *41*, 45−66.

(9) Obermayer, D.; Gutmann, B.; Kappe, C. O. Microwave Chemistry in Silicon Carbide Reaction Vials: Separating Thermal from Nonthermal Effects. *Angew. Chem.* **2009**, *121*, 8471−8474.

(10) Tsukahara, Y.; Higashi, A.; Yamauchi, T.; Nakamura, T.; Yasuda, M.; Baba, A.; Wada, Y. In Situ Observation of Nonequilibrium Local Heating as an Origin of Special Effect of Microwave on Chemistry. *J. Phys. Chem. C* **2010**, *114*, 8965−8970.

(11) Hosseini, M.; Stiasni, N.; Barbieri, V.; Kappe, C. O. Microwave-Assisted Asymmetric Organocatalysis. A Probe for Nonthermal Microwave Effects and the Concept of Simultaneous Cooling. *J. Org. Chem.* **2007**, *72*, 1417−1424.

(12) de la Hoz, A.; Diaz-Ortiz, A.; Moreno, A. Microwaves in Organic Synthesis. Thermal and Non-Thermal Microwave Effects. *Chem. Soc. Rev.* **2005**, *34*, 164−178.

(13) Binner, J.; Hassine, N.; Cross, T. The Possible Role of the Pre-Exponential Factor in Explaining the Increased Reaction Rates Observed During the Microwave Synthesis of Titanium Carbide. *J. Mater. Sci.* **1995**, *30*, 5389−5393.

(14) Wu, Y.; Gagnier, J.; Dudley, G. B.; Stiegman, A. The "Chaperone" Effect in Microwave-Driven Reactions. *Chem. Commun.* **2016**, *52*, 11281−11283.

(15) Huang, W.; Richert, R. The physics of heating by time-dependent fields: microwaves and water revisited. *J. Phys. Chem. B* **2008**, *112*, 9909−9913.

(16) Dudley, G. B.; Richert, R.; Stiegman, A. E. On the existence of and mechanism for microwave-specific reaction rate enhancement. *Chem. Sci.* **2015**, *6*, 2144−2152.

(17) Adnadjević, B.; Jovanović, J.; Potkonjak, B. A novel approach to the explanation the effect of microwave heating on isothermal kinetic of crosslinking polymerization of acrylic acid. *Rus. J. Phys. Chem. A* **2013**, *87*, 2115−2120.

(18) Vartanian, A. L.; Asatryan, A. L.; Kirakosyan, A. A. The energy-loss rate via polar-optical phonon scattering in quantum wires. *Phys. E* **2005**, *28*, 545−551.

(19) Dowgiallo, A.-M.; Knappenberger, K. L. Ultrafast electron−phonon coupling in hollow gold nanospheres. *Phys. Chem. Chem. Phys.* **2011**, *13*, 21585−21592.

(20) Li, X.-Q.; Nakayama, H.; Arakawa, Y. Phonon Bottleneck in Quantum Dots: Role of Lifetime of the Confined Optical Phonons. *Phys. Rev. B: Condens. Matter Mater. Phys.* **1999**, *59*, 5069.

(21) Dudley, G. B.; Stiegman, A. E.; Rosana, M. R. Correspondence on Microwave Effects in Organic Synthesis. *Angew. Chem., Int. Ed.* **2013**, *52*, 7918−7923.

(22) Richert, R. Nonlinear Dielectric Effects in Liquids: A Guided Tour. *J. Phys.: Condens. Matter* **2017**, *29*, 363001.

(23) Ashley, B.; Vakil, P. N.; Lynch, B.; Dyer, C. M.; Tracy, J. B.; Owens, J.; Strouse, G. F. Microwave Enhancement of Autocatalytic Growth of Nanometals. *ACS Nano* **2017**, *11*, 9957−9967.

(24) Gutmann, B.; Schwan, A. M.; Reichart, B.; Gspan, C.; Hofer, F.; Kappe, C. O. Activation and Deactivation of a Chemical Transformation by an Electromagnetic Field: Evidence for Specific Microwave Effects in the Formation of Grignard Reagents. *Angew. Chem.* **2011**, *123*, 7778−7782.

(25) Lovingood, D. D.; Strouse, G. F. Microwave Induced In-Situ Active Ion Etching of Growing InP Nanocrystals. *Nano Lett.* **2008**, *8*, 3394−3397.

(26) Lovingood, D. D.; Oyler, R. E.; Strouse, G. F. Composition Control and Localization of S2− in CdSSe Quantum Dots Grown from Li4 [Cd10Se4 (SPh) 16]. *J. Am. Chem. Soc.* **2008**, *130*, 17004−17011.

(27) Vazquez, A.; Gomez, I.; Garib, J. A.; Kharisov, B. I. Influence of Precursor and Power Irradiation on the Microwave-Assisted Synthesis of ZnS Nanoparticles. *Synth. React. Inorg. Met.-Org. Chem.* **2009**, *39*, 109−115.

(28) Gor'kov, L. P.; Eliashberg, G. Minute Metallic Particles in an Electromagnetic Field. *Sov. J. Exp. Theor. Phys.* **1965**, *21*, 940.

(29) Marquardt, P.; Nimtz, G. Size-Dependent Dielectric Response of Small Metal Particles. *Phys. Rev. B: Condens. Matter Mater. Phys.* **1991**, *43*, 14245.

(30) Troitskiy, V. N.; Domashnev, I. A.; Kurkin, E. N.; Grebtsova, O. M.; Berestenko, V. I.; Balikhin, I. L.; Gurov, S. V. Synthesis and Characteristics of Ultra-Fine Superconducting Powders in the Nb−N, Nb−N−C, Nb−Ti−N−C Systems. *J. Nanopart. Res.* **2003**, *5*, 521−528.

(31) Horikoshi, S.; Abe, H.; Sumi, T.; Torigoe, K.; Sakai, H.; Serpone, N.; Abe, M. Microwave Frequency Effect in the Formation of Au Nanocolloids in Polar and Non-Polar Solvents. *Nanoscale* **2011**, *3*, 1697−1702.

(32) Caponetti, E.; Pedone, L.; Massa, R. Microwave Radiation Effect on the Synthesis of Cadmium Sulphide Nanoparticles in Water in Oil Microemulsion: A Preliminary Study at Different Frequencies. *Mater. Res. Innovations* **2004**, *8*, 44−47.

(33) Nyutu, E. K.; Chen, C.-H.; Dutta, P. K.; Suib, S. L. Effect of Microwave Frequency on Hydrothermal Synthesis of Nanocrystalline Tetragonal Barium Titanate. *J. Phys. Chem. C* **2008**, *112*, 9659−9667.

(34) LaGrow, A. P.; Ingham, B.; Toney, M. F.; Tilley, R. D. Effect of Surfactant Concentration and Aggregation on the Growth Kinetics of Nickel Nanoparticles. *J. Phys. Chem. C* **2013**, *117*, 16709−16718.

(35) Hodak, J. H.; Martini, I.; Hartland, G. V. Spectroscopy and Dynamics of Nanometer-Sized Noble Metal Particles. *J. Phys. Chem. B* **1998**, *102*, 6958−6967.

(36) Link, S.; Burda, C.; Wang, Z. L.; El-Sayed, M. A. Electron Dynamics in Gold and Gold−Silver Alloy Nanoparticles: The Influence of a Nonequilibrium Electron Distribution and the Size Dependence of the Electron−Phonon Relaxation. *J. Chem. Phys.* **1999**, *111*, 1255−1264.

(37) Metaxas, A. C.; Meredith, R. J. *Industrial Microwave Heating*; Institute of Engineering and Technology: United Kingdom, 1983.

(38) Luty-Błocho, M.; Wojnicki, M.; Fitzner, K. Gold Nanoparticles Formation via Au(III) Complex Ions Reduction with l-Ascorbic Acid. *Int. J. Chem. Kinet.* **2017**, *49*, 789−797.

(39) Akbayrak, S.; Özkar, S. Ruthenium (0) Nanoparticles Supported on Xonotlite Nanowire: A Long-Lived Catalyst for Hydrolytic Dehydrogenation of Ammonia-Borane. *Dalton Trans.* **2014**, *43*, 1797−1805.

(40) Watzky, M. A.; Finke, R. G. Transition Metal Nanocluster Formation Kinetic and Mechanistic Studies. A New Mechanism when Hydrogen is the Reductant: Slow, Continuous Nucleation and Fast Autocatalytic Surface Growth. *J. Am. Chem. Soc.* **1997**, *119*, 10382−10400.

(41) Finney, E. E.; Finke, R. G. Nanocluster Nucleation and Growth Kinetic and Mechanistic Studies: A Review Emphasizing Transition-Metal Nanoclusters. *J. Colloid Interface Sci.* **2008**, *317*, 351−374.

DOI: 10.1021/acs.jpcc.7b11366
J. Phys. Chem. C 2018, 122, 3617−3627

(42) Polte, J. R.; Ahner, T. T.; Delissen, F.; Sokolov, S.; Emmerling, F.; Thünemann, A. F.; Kraehnert, R. Mechanism of Gold Nanoparticle Formation in the Classical Citrate Synthesis Method Derived from Coupled In Situ XANES and SAXS Evaluation. *J. Am. Chem. Soc.* **2010**, *132*, 1296−1301.
(43) Besson, C.; Finney, E. E.; Finke, R. G. A Mechanism for Transition-Metal Nanoparticle Self-Assembly. *J. Am. Chem. Soc.* **2005**, *127*, 8179−8184.
(44) Thanh, N. T.; Maclean, N.; Mahiddine, S. Mechanisms of Nucleation and Growth of Nanoparticles in Solution. *Chem. Rev.* **2014**, *114*, 7610−7630.
(45) Streszewski, B.; Jaworski, W.; Pacławski, K.; Csapó, E.; Dékány, I.; Fitzner, K. Gold Nanoparticles Formation in the Aqueous System of Gold (III) Chloride Complex Ions and Hydrazine Sulfate—Kinetic Studies. *Colloids Surf., A* **2012**, *397*, 63−72.
(46) Watzky, M. A.; Finney, E. E.; Finke, R. G. Transition-Metal Nanocluster Size vs Formation Time and the Catalytically Effective Nucleus Number: A Mechanism-Based Treatment. *J. Am. Chem. Soc.* **2008**, *130*, 11959−11969.
(47) Özkar, S.; Finke, R. G. Silver Nanoparticles Synthesized by Microwave Heating: A Kinetic and Mechanistic Re-Analysis and Re-Interpretation. *J. Phys. Chem. C* **2017**, *121*, 27643.
(48) Jędrak, J. Exact Solutions of Kinetic Equations in an Autocatalytic Growth Model. *Phys. Rev. E* **2013**, *87*, 022132.
(49) Perala, S. R. K.; Kumar, S. On the Two-Step Mechanism for Synthesis of Transition-Metal Nanoparticles. *Langmuir* **2014**, *30*, 12703−12711.
(50) Laxson, W. W.; Finke, R. G. Nucleation is Second Order: An Apparent Kinetically Effective Nucleus of Two for Ir (0) n Nanoparticle Formation from [(1, 5-COD) IrI· P2W15Nb3O62] 8− Plus Hydrogen. *J. Am. Chem. Soc.* **2014**, *136*, 17601−17615.
(51) Yang, T.-H.; Zhou, S.; Gilroy, K. D.; Figueroa-Cosme, L.; Lee, Y.-H.; Wu, J.-M.; Xia, Y. Autocatalytic Surface Reduction and its Role in Controlling Seed-Mediated Growth of Colloidal Metal Nanocrystals. *Proc. Natl. Acad. Sci. U. S. A.* **2017**, *114*, 13619.
(52) Watzky, M. A.; Finke, R. G. Nanocluster Size-Control and "Magic Number" Investigations. Experimental Tests of the "Living-Metal Polymer" Concept and of Mechanism-Based Size-Control Predictions Leading to the Syntheses of Iridium (0) Nanoclusters Centering About Four Sequential Magic Numbers. Chem. *Chem. Mater.* **1997**, *9*, 3083−3095.
(53) Özkar, S.; Finke, R. G. Iridium (0) Nanocluster, Acid-Assisted Catalysis of Neat Acetone Hydrogenation at Room Temperature: Exceptional Activity, Catalyst Lifetime, and Selectivity at Complete Conversion. *J. Am. Chem. Soc.* **2005**, *127*, 4800−4808.
(54) Ott, L. S.; Finke, R. G. Nanocluster Formation and Stabilization Fundamental Studies:† Investigating "Solvent-Only" Stabilization En Route to Discovering Stabilization by the Traditionally Weakly Coordinating Anion BF4-Plus High Dielectric Constant Solvents. *Inorg. Chem.* **2006**, *45*, 8382−8393.
(55) Richards, V. N.; Rath, N. P.; Buhro, W. E. Pathway from a Molecular Precursor to Silver Nanoparticles: The Prominent Role of Aggregative Growth. *Chem. Mater.* **2010**, *22*, 3556−3567.
(56) Harada, M.; Katagiri, E. Mechanism of Silver Particle Formation During Photoreduction Using In Situ Time-Resolved SAXS Analysis. *Langmuir* **2010**, *26*, 17896−17905.
(57) Liu, X.; Atwater, M.; Wang, J.; Dai, Q.; Zou, J.; Brennan, J. P.; Huo, Q. A study on gold nanoparticle synthesis using oleylamine as both reducing agent and protecting ligand. *J. Nanosci. Nanotechnol.* **2007**, *7*, 3126−3133.
(58) Turkevich, J.; Stevenson, P. C.; Hillier, J. A Study of the Nucleation and Growth Processes in the Synthesis of Colloidal Gold. *Discuss. Faraday Soc.* **1951**, *11*, 55−75.
(59) Kimling, J.; Maier, M.; Okenve, B.; Kotaidis, V.; Ballot, H.; Plech, A. Turkevich Method for Gold Nanoparticle Synthesis Revisited. *J. Phys. Chem. B* **2006**, *110*, 15700−15707.
(60) Liu, Q.; Gao, M.-R.; Liu, Y.; Okasinski, J. S.; Ren, Y.; Sun, Y. Quantifying the Nucleation and Growth Kinetics of Microwave Nanochemistry Enabled by in Situ High-Energy X-Ray Scattering. *Nano Lett.* **2016**, *16*, 715−720.
(61) Link, S.; El-Sayed, M. A. Size and temperature dependence of the plasmon absorption of colloidal gold nanoparticles. *J. Phys. Chem. B* **1999**, *103*, 4212−4217.
(62) Haiss, W.; Thanh, N. T.; Aveyard, J.; Fernig, D. G. Determination of size and concentration of gold nanoparticles from UV− Vis spectra. *Anal. Chem.* **2007**, *79*, 4215−4221.
(63) Breshike, C. J.; Riskowski, R. A.; Strouse, G. F. Leaving Förster Resonance Energy Transfer Behind: Nanometal Surface Energy Transfer Predicts the Size-Enhanced Energy Coupling Between a Metal Nanoparticle and an Emitting Dipole. *J. Phys. Chem. C* **2013**, *117*, 23942−23949.
(64) Huang, W.; Richert, R. Dynamics of Glass-Forming Liquids. XIII. Microwave Heating in Slow Motion. *J. Chem. Phys.* **2009**, *130*, 194509.
(65) Fröhlich, H. *Theory of Dielectrics: Dielectric Constant and Dielectric Loss*; Clarendon Press: 1958.
(66) Ashley, B.; Lovingood, D. D.; Chiu, Y.-C.; Gao, H.; Owens, J.; Strouse, G. F. Specific Effects in Microwave Chemistry Explored Through Reactor Vessel Design, Theory, and Spectroscopy. *Phys. Chem. Chem. Phys.* **2015**, *17*, 27317−27327.

DOI: 10.1021/acs.jpcc.7b11366
J. Phys. Chem. C 2018, 122, 3617−3627